MATERIALS SCIENCE

Facile full-color printing with a single transparent ink

Kaixuan Li[1,2†], Tongyu Li[3†], Tailong Zhang[1,4†], Huizeng Li[1], An Li[1,2], Zheng Li[1], Xintao Lai[1,2], Xiaoyu Hou[1,2], Yu Wang[4], Lei Shi[3], Mingzhu Li[1,5]*, Yanlin Song[1,2]*

Structural colors are promising candidates for their antifading and eco-friendly characteristics. However, high cost and complicated processing inevitably hinder their development. Here, we propose a facile full-color structural-color inkjet printing strategy with a single transparent ink from the common polymer materials. This structural color arisen from total internal reflections is prepared by digitally printing the dome-shaped microstructure (microdome) with well-controlled morphology. By controlling the ink volume and substrate wettability, the microdome color can be continuously regulated across whole visible regions. The gamut, saturation, and lightness of the printed structural-color image are precisely adjusted via the programmable arrangement of different microdomes. With the advantages of simple manufacturing and widely available inks, this color printing approach presents great potential in imaging, decoration, sensing, and biocompatible photonics.

INTRODUCTION

Color images play vitally important roles in our daily life, including printing and dyeing, decoration, optical security, and information storage (*1*–*5*). So far, the main methods to prepare the color images are based on chemical colors from dyes or pigments, which have caused serious health and pollution problems (*6*, *7*). In this case, structural colors, generated by the light interactions with specific micro- or nanostructures (*8*–*10*), are expected to be eco-friendly alternatives for their fade-resistant, brilliant, and dynamic characteristics (*11*–*15*). With the rapid development of structural-color technology, various color structures (such as gratings, thin films, photonic crystals, and local resonance structures) have been extensively studied (*16*–*20*). Moreover, as function carriers, structural-color images attract widespread explorations and have been greatly improved via the advanced nanofabrication techniques (*21*–*26*). However, the high-throughput fabrication of structural-color images is still an enormous challenge due to high requirement to integrate numerous periodic submicrometer structures or independent nanostructures in a designable way (*27*–*29*).

Preparing color images needs precise control over multicolor pixels to regulate the image parameters, including gamut, brightness, saturation, grayscale, and resolution, which determine the image quality (*23*, *30*–*32*). In commercial printing, diverse inks of different colors (at least black, magenta, cyan, and yellow colors) are ejected independently through 48 or more nozzles to satisfy the full-color coverage of pixels (*33*, *34*). Nevertheless, for structural-color pixels prepared by state-of-the-art top-down lithography and bottom-up assembly techniques, producing and integrating different pixels with fine resolutions will experience a long-time design and complicated processing procedure (*35*, *36*). Moreover, some inherent drawbacks, including high cost and limited materials (some metal plasmonic and high-index dielectric materials) in lithography as well as the necessary particle presynthesis and unpreventable defects in assembly, hinder the large-area and customized fabrication of structural-color images, thus greatly restricting them into next-generation color products (*27*, *37*). Recently, Goodling and Zarzar have demonstrated that the vivid structural colors could be produced at microscale concave interfaces and systematically proven the coloration principle of interference from total internal reflections (TIRs) (*38*, *39*), which provides the feasibility to manipulate the structural color with low-index materials (*38*–*40*). Compared with the photonic crystals based on periodic nanostructures, the structural color from TIR can be directly generated with individual microstructure without complicated particle self-assembly or polymer phase separation structures. It opens up a low-cost, high-yield, and scalable passway to achieve full structural-color printing.

Here, we develop a facile structural-color printing approach that can realize the full-color preparation of high-photorealistic images with a single transparent ink via the commercial inkjet printing technology, as shown in Fig. 1A. The transparent ink can be made in large quantities from monomer or polymer solution. When the ink droplets are printed on a hydrophobic and transparent substrate, they will retract into perfect microdomes with large curvature angles under the surface tension effect. The inverted microdomes can induce the interference color from TIR and serve as independent pixels to construct the color image. The color of each microdome, controlled by the optical path, is regulated across whole visible regions via adjusting the physical morphology, so we can easily obtain the full-color pixels with one printing nozzle and one transparent ink. Each pixel can be decoded into its corresponding printing parameter, and the full-color structural-color images are prepared by the digital programmable printer. The gamut, lightness, saturation, and grayscale of the image can be systematically controlled with single-pixel precision. In addition, this color printing method is fully compatible with the commercial printing technology and suitable for the large-area industrial production. Thus, it is highly anticipated to boost the practical applications of structural colors.

[1]Key Laboratory of Green Printing, CAS Research/Education Center for Excellence in Molecular Sciences, Institute of Chemistry, Chinese Academy of Sciences, Beijing 100190, P. R. China. [2]University of Chinese Academy of Sciences, Beijing 100049, P. R. China. [3]State Key Laboratory of Surface Physics, Key Laboratory of Micro- and Nano-Photonics Structures (Ministry of Education) and Department of Physics, Fudan University, Shanghai 200433, P. R. China. [4]School of Materials Science and Engineering, Zhengzhou University, Zhengzhou 450001, P. R. China. [5]Key Laboratory of Materials Processing and Mold of the Ministry of Education, Zhengzhou University, Zhengzhou 450002, P. R. China.
*Corresponding author. Email: mingzhu@iccas.ac.cn (M.L.); ylsong@iccas.ac.cn (Y.S.)
†These authors contributed equally to this work.

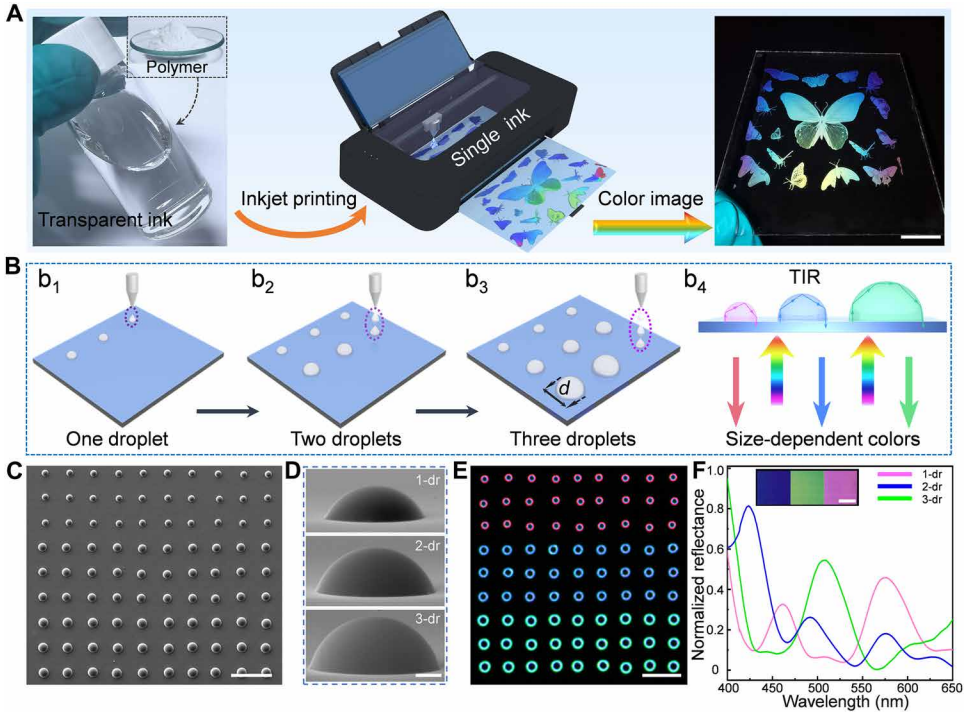

Fig. 1. Structural-color inkjet printing with a single transparent ink. (**A**) The process of structural-color printing with a single transparent polymer ink. The polymer ink can be directly fabricated by dissolving the polyacrylic acid into the mixture of water and ethylene glycol. Via inkjet printing of the polymer ink on hydrophobic substrates, the large-area color image is prepared (scale bar, 2 cm). Photo credit: K. Li, Chinese Academy of Sciences, (**B**) Schematic illustration of the D-B-D printing (b_1 to b_3) to create and integrate the different microdomes, by which the microdome diameter (*d*) can be precisely regulated. Viewing from the bare-glass (blank) side (b_4), the microdomes can exhibit size-dependent colors due to the different optical paths of TIR. (**C** and **D**) Top view (C) and cross-sectional (D) SEM images of the printed microdomes with different diameters (scale bars, 100 and 5 μm), which are prepared by one-droplet (1-dr) printing, two-droplet (2-dr) printing, and three-droplet (3-dr) printing. (**E**) Dark-field optical micrographs of the microdomes observed from the blank side (scale bar, 100 μm). (**F**) Reflection spectra of the printed structural-color panel at the macroscale. Inset is the corresponding multicolor panel composed of red, green, and blue palettes (scale bar, 1 mm), which are achieved by one-droplet, two-droplet, and three-droplet printing.

RESULTS

Structural-color printing with a single transparent polymer ink

We developed an on-demand and in situ strategy named droplet-by-droplet (D-B-D) printing to fabricate and integrate the color microdomes with a single transparent ink (Fig. 1B). To ensure the microdome with high *H*/*D* (height-to-diameter) ratio, we printed the polymer droplets on hydrophobic glass. On the hydrophobic substrate with the ink contact angle of 82.5°, the deposited droplets can retract quickly with the continuous sliding of three-phase contact lines (TCLs) and are molded into microdomes under hydrophobic effect (see figs. S1 and S2). Larger microdomes were fabricated by depositing another droplet in situ. The two droplets could merge and be shaped into the enlarged microdome (see figs. S3 and S4). Thus, via the wettability control and precise positioning, the microdomes with different sizes can be precisely prepared and integrated on the same substrate using one printing nozzle. With the incidence of collimation light from the bare glass (blank) side to the microdome patterned (printed) side, these inverted microdomes are illuminated independently and exhibit vivid size-dependent colors.

By using the 1-pl cartridge, we successfully fabricated the microdomes with diameters of about 16.2, 20.3, and 23.5 μm via one-droplet, two-droplet, and three-droplet printing, respectively (Fig. 1C). From the cross-sectional scanning electron microscopy (SEM) images in Fig. 1D, it is clear that the microdome morphology is symmetrical with smooth surface. The inverted microdome induces the TIR-based color. Different microdomes can lead to discrepant TIR and interference paths, resulting in the size-dependent coloration. Figure 1E presents the inverted microdomes with red, blue, and green colors, corresponding to the diameters of 16.2, 20.3, and 23.5 μm, respectively. The microdome arrays via large-area inkjet printing own a narrow size distribution (see fig. S5), ensuring the color uniformity in macroscale. Thus, the uniform red, green, and blue structural-color films could be easily prepared by controlling the number of ink droplet (Fig. 1F). We observed the real-time coloration of the ink droplet during printing (see figs. S6 and S7 and movie S1), which clearly proves the direct generation and high-precision manipulation of the color microdomes.

Facile preparation of the full-color microdomes

The morphology of each microdome, represented by the diameter (*d*) and the curvature angle (θ_{cua}), controls the reflected color. By adjusting the substrate wettability, the curvature angle of the printed microdome can be regulated. We prepared the substrates with different wettability to control the θ_{cua} (Fig. 2A and fig. S8). θ_{cua} can be increased with the enhancement of substrate hydrophobicity. Furthermore, the curvature angles of different microdomes are basically constant on the same substrate because of the homogeneous

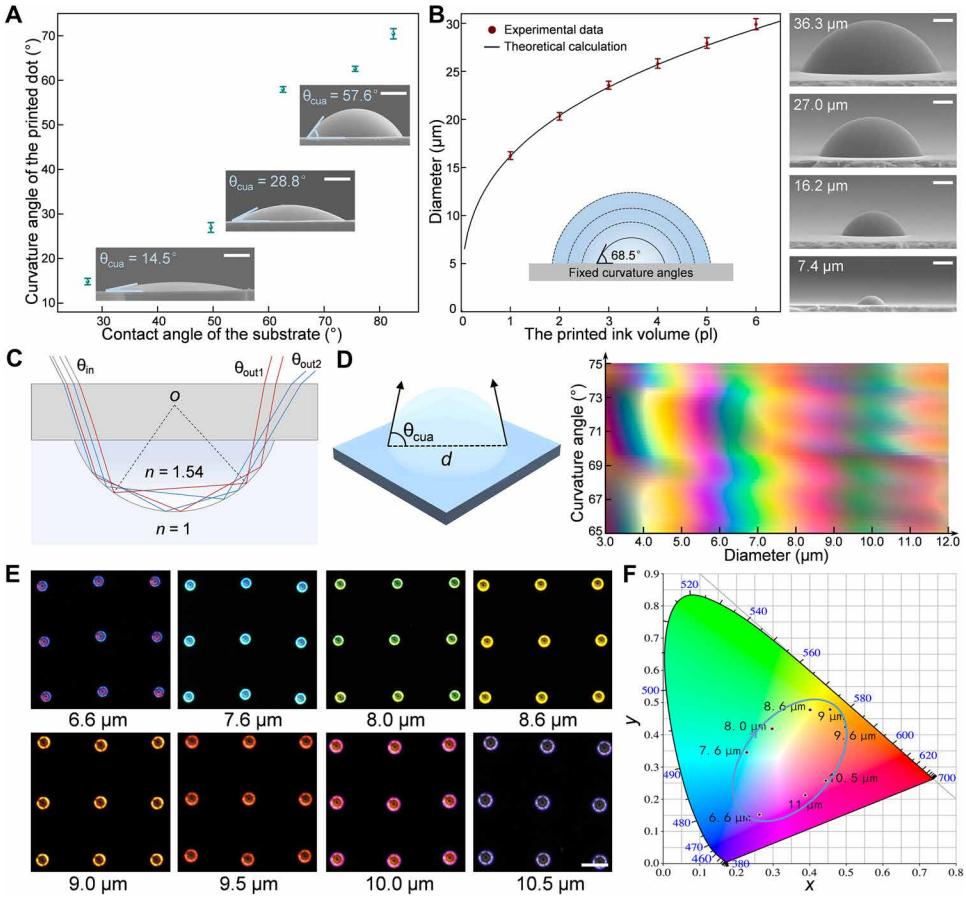

Fig. 2. Facile preparation of the full-color microdomes. (**A**) The regulation of θ_{cua} controlled by the substrate wettability (represented by the ink contact angle). Insets are the cross-sectional SEM images of the printed microdomes, showing the increased θ_{cua} with the enhancement of substrate hydrophobicity (scale bars, 5 μm). (**B**) Regulation of the microdome diameter on the hydrophobic substrate by adjusting the ink volume. For the homogeneous hydrophobicity, the microdomes can be enlarged with a fixed curvature angle (shown in the inset sketch map) as the ink volume increases. Right cross-sectional SEM images show the microdomes with different diameters (scale bars, 5 μm). (**C**) Schematic diagram of the optical ray paths propagating along the microdome-based concave interface, at which TIRs will happen. (**D**) The color simulation regulated by the curvature angle (θ_{cua}) and diameter (*d*), which are two main factors to control the reflected colors (proven in Eq. 2). With the change of θ_{cua} and *d*, full-color variation is achieved. (**E**) Dark-field optical micrographs of the printed color microdomes. Full-color microdomes are presented with the change of diameter (scale bar, 20 μm). (**F**) CIE chromaticity coordinates of the color evolution in (E).

hydrophobicity, which ensures the on-chip curvature uniformity (see fig. S9). For the fixed curvature angle, the microdome diameter (*d*) is adjusted by the ink volume (V_i) as

$$\pi d^3 = V_i \times A \times X \quad (1)$$

A is determined by θ_{cua} (about 68.5°), as $A = \frac{24(\sin\theta_{cua})^3}{(2+\cos\theta_{cua})(1-\cos\theta_{cua})^2}$ (see fig. S10), and X is the retention rate controlled by ink evaporation during processing (about 0.68) (see fig. S11). Thus, the microdome diameter can be calculated as $d = 16.39\sqrt[3]{V_i}$ and precisely regulated from several micrometers to tens of micrometers by controlling the substrate wettability and ink volume (Fig. 2B).

To obtain the full-color microdomes, we systematically studied the relationship between the reflected color and microdome morphology. Basically, white light is a combination of electromagnetic waves with varying frequencies. It will be splitted into separated waves with the light hitting the microdome-patterned substrate. At the concave polymer-air interfaces, TIR will occur because of the contrast transition of refractive index (n_m = 1.54 and n_a = 1). TIR can change the phase and enhance the reflected intensity. After multiple TIRs, the waves are emitted from the microdome. The waves propagating along different trajectories but emitting at the same angles (θ_{out}) will take interference and result in the coloration (Fig. 2C). We theoretically simulated the interference of waves to trace all allowed trajectories and calculated the total phase variation for each path according to the coloration theory in multiphase microdroplets (*38*) (see the "Numerical simulations" section). On the basis of the model, the color of each microdome was calculated with the change *d* and θ_{cua} of each microdome (Fig. 2D). It proves only that, when θ_{cua} is larger than 46°, the color can be created (see fig. S12). At each fixed θ_{cua}, the microdome color could be regulated as the diameter changed, and the full colors across the whole visible region were mapped with the diameter changed from 3 to 12 μm. In the experiment, as the diameter was adjusted from 6.6 to 11 μm, the observed colors of the microdomes were shifted from blue to red and then to blue again (Fig. 2E), matching well with the simulated results and covering about 72% of the standard red green blue

(sRGB) color gamut (Fig. 2F). We also performed the spectrum measurements on structural-color films composed of different microdomes and compared them with the simulated spectra of individual microdomes. The shift of interference peaks in the simulated and measured spectra exhibited a similar trend with the change of microdome diameter (see fig. S13). The consistent experiment results with the numerical simulation indicate that the printed structural color can be predicted by the quantitative calculation, which enables the digital full-color designing and printing.

Programmable distribution of the different color microdomes

With our printing method, the spatial distribution of different color microdomes is programmable to fabricate microscale multicolor patterns (see fig. S14) and achieve color mixing (see fig. S15). Color mixing, obtained by spatially distributing separated subpixels into a composite pixel, can produce almost unlimited blend colors and help to cover the RGB color gamut continuously (*41*, *42*). By D-B-D printing, we can integrate diverse primary subpixels and edit the subpixels at will to design composite pixels (see movie S2). Figure 3A shows the color mixing based on two primary subpixels (with the chromaticity values of $x = 0.4506$ and $y = 0.3418$, and the values of $x = 0.1847$ and $y = 0.2169$). With the change of the subpixels in the composite pixel, the chromaticity values of the blend color were correspondingly converted from I (0.4506, 0.3418), II (0.4230, 0.3369), III (0.3864, 0.3306), IV (0.3209, 0.3076), to V (0.1847, 0.2169) (see fig. S16). The characteristic reflection peaks in the spectra were shifted with the regulation of the subpixels, which explains the variation of blend colors (Fig. 3B). As our color printing method could manipulate the pixels at will, it is feasible to fabricate diverse blend colors. As a proof of concept, blend colors such as brown, raw umber, and cool gray were prepared experimentally (Fig. 3C).

Because the printed microdome is colored as an independent pixel, the lightness of the palette can be regarded as the summation of the microdomes in the whole region. It can be modulated by the microdome density or the printing resolution, which is performed by controlling the pitch (p) (Fig. 3D). By regulating the pitch, the printing resolutions from 842 dpi × dpi to 508 dpi × dpi were obtained (see fig. S17). In the region of 162 μm by 162 μm, the microdome density was adjusted from 16 to 9 with the pitch changed from 40 to 60 μm (Fig. 3E). We prepared six structural-color palettes composed of the microdomes with different densities on

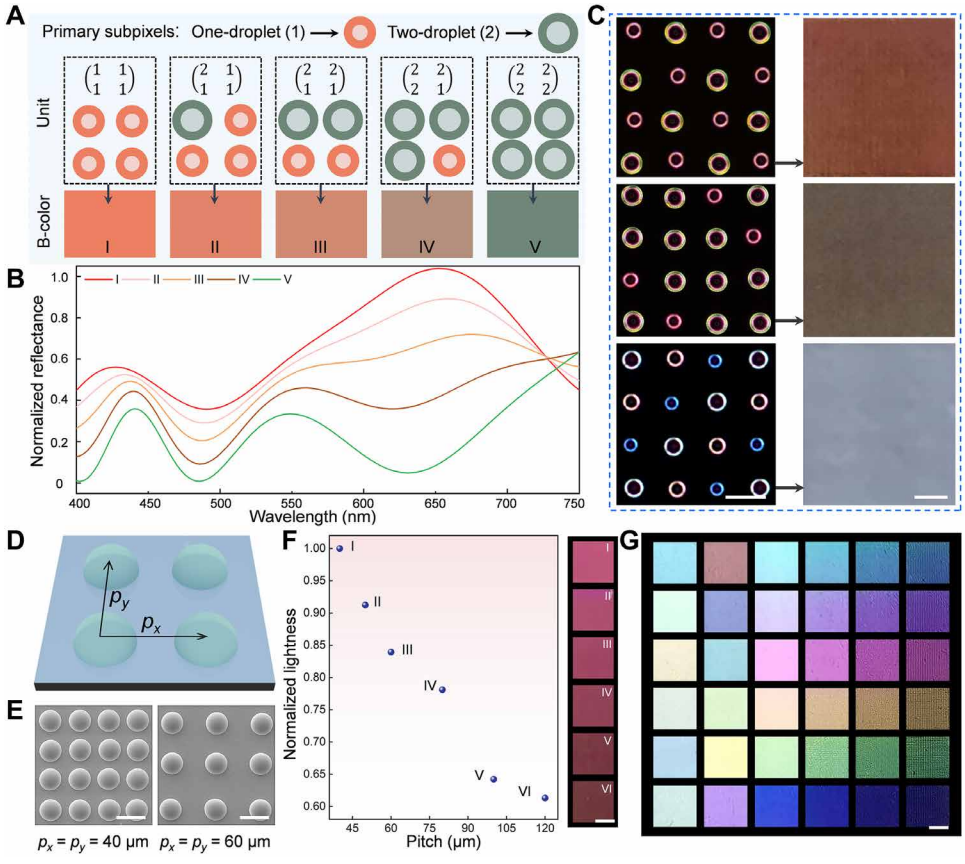

Fig. 3. Programmable distribution of the color microdomes. (**A**) The creation of blend structural colors (b-colors) by regulating the distribution of different microdomes in the composite pixels. (**B**) The reflection spectra of different b-colors corresponding to (A). (**C**) The printed b-colors composed of different composite pixels. Left dark-field micrographs are the composite pixels and right images are the resulted b-colors (scale bars, 60 μm and 0.5 mm). (**D**) Pitch regulation of the color microdomes. Pitch (p_x and p_y) is the central distance of the neighboring microdomes. Here, p_x is equal to p_y. By controlling the pitch, the pixel density can be regulated. (**E**) Top view: SEM images of printed microdome pixels with different periodicities (scale bars, 40 μm). (**F**) The lightness regulation of the color palettes by changing the pitch from 40 μm (I) to 120 μm (VI) (scale bar, 2 mm). (**G**) The printed full-color panel composed of 36 structural-color palettes (scale bar, 2 mm). The various color palettes with controlled gamut and lightness are printed on one substrate. Photo credit: K. Li, Chinese Academy of Sciences.

one substrate and collected their reflection images simultaneously. From the images, the lightness distribution could be analyzed and calculated (see fig. S18), which demonstrated that the lightness of the palettes could be continuously altered by regulating the microdome density (Fig. 3F). Thus, we can print the full-color panel with wide color gamut and adjustable lightness (Fig. 3G), which proves the powerful capability of our approach in full-color printing.

Generous fabrication of exquisite structural-color images

For our color printing strategy, a single transparent polymer ink is enough to achieve full-color printing. As we can prepare well-controlled color microdomes that are consistent with the numerical simulation, the structural-color images can be precisely designed and prepared by the computer program. As shown in Figure 4A, we first obtained the full-color library via computer simulation. Each color corresponds to its fixed printing parameter. When the refractive index of the ink is fixed, we just need to input the digital photo into the computer. The computer will decode the photo information into designed microdome arrays and send the instructions including the position, diameter, and periodicity to the printer to manufacture them. Without any complicated design or tedious process, the structural-color images can be fabricated facilely and efficiently. Figure 4B shows various structural-color images including those of a green reptile, pink follower, and yellow bird, which are composed of the microdomes with different diameters. Besides the images, we also prepared multicolor images with different hues such as those of a colorful peacock, pseudo-homochromatic number 12, and two-dimensional codes (Fig. 4C). Furthermore, these color images could be directly recorded with a smart phone, which presents the great prospects in practical applications (see fig. S19).

Besides the elementary images, elaborate structural-color portrait images were also prepared. The manufacture of portrait images has high requirements for gamut, saturation, lightness, and grayscale gradient, which is still a challenge for current structural-color techniques. In particular, the grayscale is vital to avoid image distortion, which can be converted from sRGB color space, as $I_{gray} = (0.3 \times R) + (0.59 \times G) + (0.11 \times B)$ (see fig. S20). With our printing method, the grayscale of each microdome could be continuously regulated from 0.152 to 0.803 with the diameter changed from 15 to 30 μm (Fig. 4D). By regulating the distribution of different microdomes, the grayscale gradient and visual effects of the structural-color images were controlled (see fig. S21). In memory of the milestone work of Isaac Newton in light dispersion, one of his grayscale portraits is taken as the printed image. Figure 4E shows the regulation of the designed grayscale images and corresponding printed color images. It is clear that the designed image can be transformed from distorted into realistic state when the grayscale distribution in the pupil region is lower than the area around the eye. In the experiment, by designing the distribution of different microdomes, we obtained the printed images with contrast visual effects.

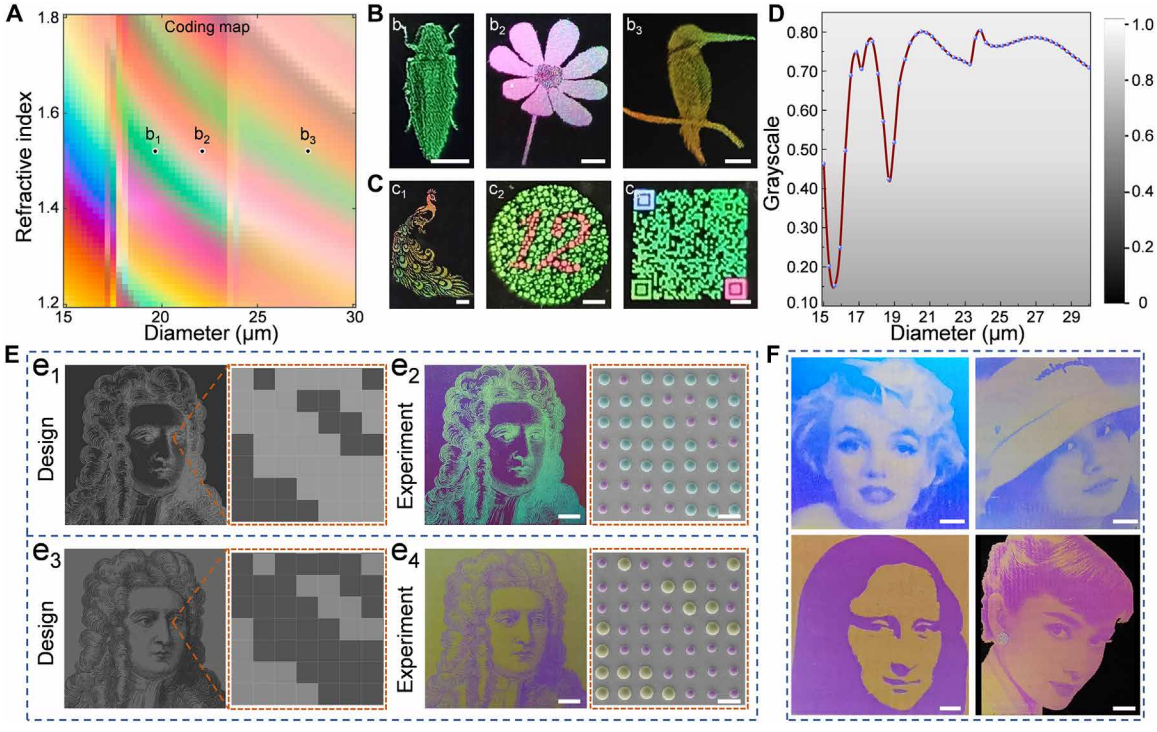

Fig. 4. Generous fabrication of exquisite structural-color images. (**A**) The simulated color map controlled by the ink refractive index and microdome diameter. With the map, a computer can extract the printing parameters and prepare the structural-color image directly. The spots in the map (b_1, b_2, and b_3) are the printing parameters corresponding to (B). (**B**) Photographs of the pure-color images, including the green reptile (b_1), pink follower (b_2), and yellow bird (b_3) (scale bars, 2 mm). (**C**) Photographs of the multicolor images, including the colorful peacock (c_1), pseudo-homochromatic number 12 (c_2), and two-dimensional codes (c_3) (scale bars, 2 mm). (**D**) The grayscale variation of microdomes with the change of diameter. (**E**) The designed grayscale and experimental colorful images of Isaac Newton's portrait (scale bars, 5 mm). The enlarged parts are the detailed grayscale distribution (e_1 and e_3) and the top view marked SEM images of the printed microdomes (e_2 and e_4) (scale bars, 40 μm). The portrait image can present contrast visual effects for the different distributions of microdomes. (**F**) Diverse printed realistic images including Marilyn Monroe, ordinary girl, Mona Lisa, and Audrey Hepburn. They can all be prepared with very high fidelity (scale bars, 5 mm). Photo credit: K. Li, Chinese Academy of Sciences.

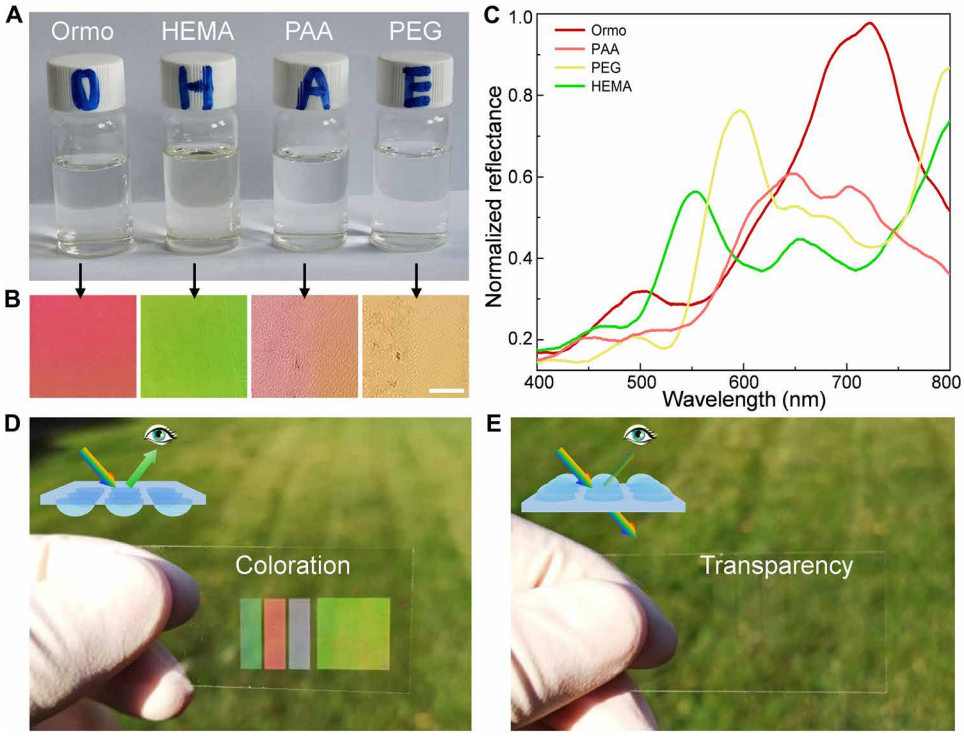

Fig. 5. Various inks for structural-color printing and the optical Janus property. (**A** and **B**) The various transparent polymer inks (A) that can be applied to the structural-color printing (B) (scale bar, 2 mm), including Ormo (a commercial polymer ink), HEMA (hydroxyethyl methacrylate), PAA (polyacrylic acid), and PEG. (**C**) The reflectance spectra of the printed structural-color films with different inks. (**D** and **E**) The optical Janus property of coloration and transparency of the printed structural-color panel viewing from the bare unpatterned (blank) side (D) and microdome patterned (printed) side (E). Insets are the schematic diagrams of the different observing modes. The structural-color panel can become almost transparent from coloration when it is observed from the printed side. Photo credit: K. Li, Chinese Academy of Sciences.

Because the grayscale gradient of the structural-color images could be precisely controlled, various high-photorealistic structural-color images were fabricated generally (Fig. 4F).

DISCUSSION

In conclusion, we have demonstrated an efficient and general structural-color printing approach with a single transparent ink through the commercial digital inkjet printing technology. The vivid structural color resulted from the microscale concave interface is finely manipulated by controlling the substrate wettability and the printed ink volume. The gamut, lightness, saturation, and grayscale of the structural-color images can be easily and precisely regulated via controlling the microdome distribution.

In addition, many commercial polymer materials such as hydroxyethyl methacrylate, polyacrylic acid, and polyethylene glycol (PEG) can be made into ink and applied to the structural-color printing (Fig. 5, A to C). Furthermore, the printed structural-color palette can present the angle-dependent characteristics. The change of illumination or viewing conditions will affect the TIR paths and interference rays, leading to different reflection colors (see fig. S22). By combining the inherent properties of the polymer material such as shape memory and smart response with the iridescent structural color, more interesting features and functions are expected. Last but not least, because of the special asymmetric optical and morphological characteristics of the printed structural-color panel, it can exhibit the optical Janus property of coloration and transparency when it is observed from different sides (Fig. 5, D and E), which is highly promising in the applications of smart window, dynamic display, anticounterfeiting technology, and colorimetric sensor. Therefore, we believe that the color printing method can greatly promote practical applications of structural colors.

MATERIALS AND METHODS

Preparing polymer inks

The polymer ink (InkOrmo, Micro Resist Technology, Germany) with the refractive index of 1.54 was purchased from Suzhou Yancai Micro and Nano Technology Co. Ltd. The homemade polymer ink of hydroxyethyl methacrylate was prepared through mixing monomer, prepolymer, reactive dilute, photo initiator, and other additions. Polyacrylic acid (PAA) polymer ink was prepared by mixing PAA [molecular weight (Mw), 1800; Sigma-Aldrich] with deionized water/ethylene glycol mixed solvent (with a mass ratio of 4:6). The concentration of solute was maintained at 5 to 16 weight % (wt %). PEG polymer ink was prepared by mixing PEG (Mw, 8000; Sigma-Aldrich) with deionized water/ethylene glycol mixed solvent (with a mass ratio of 4:6). The concentration of solute was maintained at 5 to 15 wt %.

Fabricating transparent and hydrophobic substrates

Glass slides were sequentially washed with ethanol, acetone, and deionized water and then blow-dried with nitrogen. To increase the surface energy, the transparent glasses were treated with air plasma

(DT-02S, OPS Plasma Technology Co. Ltd., China) at 120 W for 180 s. Then, the surface of slides became sufficiently hydrophilic. After surface-modified with 1*H*,1*H*,2*H*,2*H*-perfluorodecyltrimethoxysilane by chemical vapor deposition at 80°C for 2 hours, the transparent slides with low surface energy were fabricated. Polydimethylsiloxane substrate (Sylgard 184 silicone elastomer kit, Dow) was mixed with the curing agent (10:1 w/w) and stirred by a mechanical stirrer for 5 min. Then, the liquid was poured over a flat petri dish and cured at 70°C for at least 2 hours.

Drop impact process

The polymer droplet of Ormo is formed by slowly squeezing the nozzle until the droplet detaches under gravity, with an initial speed of zero. Impact speed is adjusted by regulating the height of the nozzle. The diameter of the polymer droplets is 2.1 mm. The impact behaviors are recorded using high-speed cameras: Phantom V12.1 and Phantom VEO401L (Vision Research Inc.).

Printing process

We used the inkjet printing (DMP-2831, Dimatix Fujifilm, Japan and Microplotter II, Sonoplot, American) technology to prepare the microdomes by printing the polymer ink on the hydrophobic substrate through a computer-predefined design. When the ink droplet containing the solute is drying on the hydrophobic surface of an unheated substrate, the solute within the droplet will move inward carried by the sliding TCL, inducing the formation of domed microstructures. Heating the substrate can increase the evaporation speed and lead to the enhanced evaporation near the drop's edge, which will increase the transfer of solute from the center to the contact line and hinder the movement of the TCL, resulting in the decrease of *H/D* ratio (*43*, *44*). To ensure the free movement of TCL and prepare the microdome with high *H/D* ratio, the substrate temperature during the structural-color printing was kept at about 25°C. Microdomes with different diameters were well controlled by regulating the volume of ink droplet.

Numerical simulations

The interference of waves can be theoretically modeled to trace all allowed trajectories and to calculate the total phase variation for each path, according to the proved TIR theory in multiphase microdroplets (*38*). When a monochromatic light enters the microdome (whose diameter is d and refractive index is n_1) with an incident angle θ_{in}, the intensity I at observation direction θ_{out} can be described, by counting the number of total reflections (m) that happen in the propagation, as

$$I = \sum_{p=\pm 1} \left| \sum_{m_{min,p}}^{m_{max,p}} A_m(a_{m,p})\, r_m^m\left(a_{m,p}, \frac{n_1}{n_0}\right) \exp\left[i\frac{2\pi}{\lambda_0} \cdot n_1 m d \cos(a_{m,p}) \right] \right|^2 \quad (2)$$

where $a_{m,p} = \pi/2 - (\pi - \theta_{in} + \theta_{out})/2m$ is the local incidence angle for each trajectory; λ_0 is the wavelength of light in air, n_0 is refractive index of air; $A_m = \sqrt{(\cos(a_{m,p})/m)}$ is the amplitude scaling factor related to angular density of ray; r_m is the complex Fresnel reflection coefficient, which determines phase change in each reflection; and the exponential term corresponds to the phase change caused by propagation in the microdome, where $n_1 md \cos(a_{m,p})$ is the optical path of each trajectory, which is controlled by the diameter (d) and curvature angle (θ_{cua}) of the microdome. For a given pair of incident angle θ_{in} and observing angle θ_{out}, there is a pair of possible trajectories represented by index p. Because the incident lights of two trajectories strike at two opposite parts of the microdome and propagate in different directions, their interference will not occur and the lights of the two trajectories are summed up incoherently to obtain the final intensity.

The color simulation of the independent microdome was implemented by MATLAB. The calculated intensity spectrum for each value can then be converted to CIE XYZ color coordinates using the color-matching functions. A micodome is illuminated by multiple rays with the same incident angle θ_{in} and different azimuthal angles ϕ. For the incident lights with different azimuthal angles to be incoherent, these lights contribute to the observed intensity incoherently after propagating in the microdome. According to the rotational symmetry, the intensity can be alternatively calculated using single light incidence condition

$$I(\theta_{out,air}) = \int_0^{2\pi} I(\theta_{out,air}, \phi_{out})\, d\phi_{out} \quad (3)$$

Here, using Snell's law, the incident/observed angle in medium air (θ_{out}) can be easily calculated according to that

$$n_0 \theta_{out,air} = n_1 \theta_{out} \quad (4)$$

The spectra are lastly averaged from 85° to 95° to approximate the experimental reception. The calculated spectra are then converted into XYZ/RGB coordinates using CIE standard color matching functions to compare with the experimental results. The CIE coordinates were then converted to sRGB to be displayed. The MATLAB code used to implement the model is downloaded from https://github.com/snnagel/Structural-color-by-Cascading-TIR (*38*).

Characterizations

Contact angles were measured using a contact angle measurement device (OCA20, Data Physics, Germany) with the polymer droplet (2 ml). The printed microstructures were characterized by field-emission SEM (JEOL, JSM-7500F, Japan) at an accelerating voltage of 5.0 kV. The optical micrographs of each pixel were recorded by a dark-field microscope (Nikon ECLIPSE Ti). The reflection spectra were measured by an angle-resolved spectrum system (ideaoptics, China) equipped with a high-sensitive spectrometer (NOVA, ideaoptics, China). The reflection optical graphs were captured using a Canon EOS 7D camera and a smart phone Honor V30 PRO.

SUPPLEMENTARY MATERIALS

Supplementary material for this article is available at https://science.org/doi/10.1126/sciadv.abh1992

REFERENCES AND NOTES

1. F. Neubrech, X. Duan, N. Liu, Dynamic plasmonic color generation enabled by functional materials. *Sci. Adv.* **6**, eabc2709 (2020).
2. W. Fan, J. Zeng, Q. Gan, D. Ji, H. Song, W. Liu, L. Shi, L. Wu, Iridescence-controlled and flexibly tunable retroreflective structural color film for smart displays. *Sci. Adv.* **5**, eaaw8755 (2019).
3. H. S. Kang, S. W. Han, C. Park, S. W. Lee, H. Eoh, J. Baek, D.-G. Shin, T. H. Park, J. Huh, H. Lee, D.-E. Kim, D. Y. Ryu, E. L. Thomas, W.-G. Koh, C. Park, 3D touchless multiorder reflection structural color sensing display. *Sci. Adv.* **6**, eabb5769 (2020).
4. J. Oh, D. Baek, T. K. Lee, D. Kang, H. Hwang, E. M. Go, I. Jeon, Y. You, C. Son, D. Kim, M. Whang, K. Nam, M. Jang, J.-H. Park, S. K. Kwak, J. Kim, J. Lee, Dynamic multimodal holograms of conjugated organogels via dithering mask lithography. *Nat. Mater.* **20**, 385–394 (2021).

5. L. Qin, X. Liu, K. He, G. Yu, H. Yuan, M. Xu, F. Li, Y. Yu, Geminate labels programmed by two-tone microdroplets combining structural and fluorescent color. *Nat. Commun.* **12**, 699 (2021).
6. A. Bafana, S. S. Devi, T. Chakrabarti, Azo dyes: Past, present and the future. *Environ. Rev.* **19**, 350–371 (2011).
7. S. Radoor, J. Karayil, J. Parameswaranpillai, S. Siengchin, Removal of anionic dye Congo red from aqueous environment using polyvinyl alcohol/sodium alginate/ZSM-5 zeolite membrane. *Sci. Rep.* **10**, 15452 (2020).
8. N. Vogel, S. Utech, G. T. England, T. Shirman, K. R. Phillips, N. Koay, I. B. Burgess, M. Kolle, D. A. Weitz, J. Aizenberg, Color from hierarchy: Diverse optical properties of micron-sized spherical colloidal assemblies. *Proc. Natl. Acad. Sci. U.S.A.* **112**, 10845–10850 (2015).
9. A. Espinha, C. Dore, C. Matricardi, M. I. Alonso, A. R. Goñi, A. Mihi, Hydroxypropyl cellulose photonic architectures by soft nanoimprinting lithography. *Nat. Photonics* **12**, 343–348 (2018).
10. M. Lopez-Garcia, N. Masters, H. E. O'Brien, J. Lennon, G. Atkinson, M. J. Cryan, R. Oulton, H. M. Whitney, Light-induced dynamic structural color by intracellular 3D photonic crystals in brown algae. *Sci. Adv.* **4**, eaan8917 (2018).
11. Y. Zhao, Z. Xie, H. Gu, C. Zhu, Z. Gu, Bio-inspired variable structural color materials. *Chem. Soc. Rev.* **41**, 3297–3317 (2012).
12. A. G. Dumanli, T. Savin, Recent advances in the biomimicry of structural colours. *Chem. Soc. Rev.* **45**, 6698–6724 (2016).
13. S. Tadepalli, J. M. Slocik, M. K. Gupta, R. R. Naik, S. Singamaneni, Bio-optics and bio-inspired optical materials. *Chem. Rev.* **117**, 12705–12763 (2017).
14. F. Fu, L. Shang, Z. Chen, Y. Yu, Y. Zhao, Bioinspired living structural color hydrogels. *Sci. Robot.* **3**, eaar8580 (2018).
15. W.-J. Joo, J. Kyoung, M. Esfandyarpour, S.-H. Lee, H. Koo, S. Song, Y.-N. Kwon, S. H. Song, J. C. Bae, A. Jo, M.-J. Kwon, S. H. Han, S.-H. Kim, S. Hwang, M. L. Brongersma, Metasurface-driven OLED displays beyond 10,000 pixels per inch. *Science* **370**, 459–463 (2020).
16. M. M. Ito, A. H. Gibbons, D. Qin, D. Yamamoto, H. Jiang, D. Yamaguchi, K. Tanaka, E. Sivaniah, Structural colour using organized microfibrillation in glassy polymer films. *Nature* **570**, 363–367 (2019).
17. B. B. Patel, D. J. Walsh, D. H. Kim, J. Kwok, B. Lee, D. Guironnet, Y. Diao, Tunable structural color of bottlebrush block copolymers through direct-write 3D printing from solution. *Sci. Adv.* **6**, eaaz7202 (2020).
18. J. Ge, Y. Yin, Responsive photonic crystals. *Angew. Chem. Int. Edit.* **50**, 1492–1522 (2011).
19. G. Qu, W. Yang, Q. Song, Y. Liu, C.-W. Qiu, J. Han, D.-P. Tsai, S. Xiao, Reprogrammable meta-hologram for optical encryption. *Nat. Commun.* **11**, 5484 (2020).
20. P. Mao, C. Liu, F. Song, M. Han, S. A. Maier, S. Zhang, Manipulating disordered plasmonic systems by external cavity with transition from broadband absorption to reconfigurable reflection. *Nat. Commun.* **11**, 1538 (2020).
21. K. Kumar, H. Duan, R. S. Hegde, S. C. W. Koh, J. N. Wei, J. K. W. Yang, Printing colour at the optical diffraction limit. *Nat. Nanotechnol.* **7**, 557–561 (2012).
22. X. Zhu, W. Yan, U. Levy, N. A. Mortensen, A. Kristensen, Resonant laser printing of structural colors on high-index dielectric metasurfaces. *Sci. Adv.* **3**, e1602487 (2017).
23. H. Kim, J. Ge, J. Kim, S.-e. Choi, H. Lee, H. Lee, W. Park, Y. Yin, S. Kwon, Structural colour printing using a magnetically tunable and lithographically fixable photonic crystal. *Nat. Photonics* **3**, 534–540 (2009).
24. X. Zhu, C. Vannahme, E. Højlund-Nielsen, N. A. Mortensen, A. Kristensen, Plasmonic colour laser printing. *Nat. Nanotechnol.* **11**, 325–329 (2016).
25. W. Yang, S. Xiao, Q. Song, Y. Liu, Y. Wu, S. Wang, J. Yu, J. Han, D.-P. Tsai, All-dielectric metasurface for high-performance structural color. *Nat. Commun.* **11**, 1864 (2020).
26. Y. Liu, H. Wang, J. Ho, R. C. Ng, R. J. H. Ng, V. H. Hall-Chen, E. H. H. Koay, Z. Dong, H. Liu, C.-W. Qiu, J. R. Greer, J. K. W. Yang, Structural color three-dimensional printing by shrinking photonic crystals. *Nat. Commun.* **10**, 4340 (2019).
27. A. Kristensen, J. K. W. Yang, S. I. Bozhevolnyi, S. Link, P. Nordlander, N. J. Halas, N. A. Mortensen, Plasmonic colour generation. *Nat. Rev. Mater.* **2**, 16088 (2016).
28. S. Daqiqeh Rezaei, Z. Dong, J. Y. E. Chan, J. Trisno, R. J. H. Ng, Q. Ruan, C.-W. Qiu, N. A. Mortensen, J. K. W. Yang, Nanophotonic structural colors. *ACS Photonics* **8**, 18–33 (2021).
29. E. S. Goerlitzer, R. N. Klupp Taylor, N. Vogel, Bioinspired photonic pigments from colloidal self-assembly. *Adv. Mater.* **30**, 1706654 (2018).
30. M. K. Hedayati, M. Elbahri, Review of metasurface plasmonic structural color. *Plasmonics* **12**, 1463–1479 (2017).
31. H. Liu, W. Dong, H. Wang, L. Lu, Q. Ruan, Y. S. Tan, R. E. Simpson, J. K. W. Yang, Rewritable color nanoprints in antimony trisulfide films. *Sci. Adv.* **6**, eabb7171 (2020).
32. J. S. Lee, J. Y. Park, Y. H. Kim, S. Jeon, O. Ouellette, E. H. Sargent, D. H. Kim, J. K. Hyun, Ultrahigh resolution and color gamut with scattering-reducing transmissive pixels. *Nat. Commun.* **10**, 4782 (2019).
33. F. De Voeght, E. Van Thillo, Inkjet printing methods and inkjet ink sets. U.S. Patent 8,282,197[P] (2012).
34. J. M. Serra, N. M. Moroney, High-resolution inkjet printing using color drop placement on every pixel row during a single pass. U.S. Patent 6,367,908[P] (2002).
35. J. Hou, M. Li, Y. Song, Patterned Colloidal Photonic Crystals. *Angew. Chem. Int. Edit.* **57**, 2544–2553 (2018).
36. M. Kolle, S. Lee, Progress and opportunities in soft photonics and biologically inspired optics. *Adv. Mater.* **30**, 1702669 (2018).
37. J. Ren, Y. Wang, Y. Yao, Y. Wang, X. Fei, P. Qi, S. Lin, D. L. Kaplan, M. J. Buehler, S. Ling, Biological material interfaces as inspiration for mechanical and optical material designs. *Chem. Rev.* **119**, 12279–12336 (2019).
38. A. E. Goodling, S. Nagelberg, B. Kaehr, C. H. Meredith, S. I. Cheon, A. P. Saunders, M. Kolle, L. D. Zarzar, Colouration by total internal reflection and interference at microscale concave interfaces. *Nature* **566**, 523–527 (2019).
39. A. E. Goodling, S. Nagelberg, M. Kolle, L. D. Zarzar, Tunable and responsive structural color from polymeric microstructured surfaces enabled by interference of totally internally reflected light. *ACS Macro Lett.* **2**, 754–763 (2020).
40. K. H. Ku, B. R. McDonald, H. Vijayamohanan, C. A. Zentner, S. Nagelberg, M. Kolle, T. M. Swager, Dynamic coloration of complex emulsions by localization of gold rings near the triphase junction. *Small* **17**, 2007507 (2021).
41. A. L. Holsteen, A. F. Cihan, M. L. Brongersma, Temporal color mixing and dynamic beam shaping with silicon metasurfaces. *Science* **365**, 257–260 (2019).
42. X. Zang, F. Dong, F. Yue, C. Zhang, L. Xu, Z. Song, M. Chen, P.-Y. Chen, G. S. Buller, Y. Zhu, S. Zhuang, W. Chu, S. Zhang, X. Chen, Polarization encoded color image embedded in a dielectric metasurface. *Adv. Mater.* **30**, 1707499 (2018).
43. D. Soltman, V. Subramanian, Inkjet-printed line morphologies and temperature control of the coffee ring effect. *Langmuir* **24**, 2224–2231 (2008).
44. N. D. Patil, P. G. Bange, R. Bhardwaj, A. Sharma, Effects of substrate heating and wettability on evaporation dynamics and deposition patterns for a sessile water droplet containing colloidal particles. *Langmuir* **32**, 11958–11972 (2016).
45. H. Li, W. Fang, Z. Zhao, A. Li, Z. Li, M. Li, Q. Li, X. Feng, Y. Song, Droplet precise self-splitting on patterned adhesive surfaces for simultaneous multidetection. *Angew. Chem. Int. Edit.* **59**, 10535–10539 (2020).
46. K.-C. Park, P. Kim, A. Grinthal, N. He, D. Fox, J. C. Weaver, J. Aizenberg, Condensation on slippery asymmetric bumps. *Nature* **531**, 78–82 (2016).
47. S. Li, Z. Y. Wei, J. Du, P. Wei, Z. X. Hou, B. H. Lu, The fusion process of successive droplets impinging onto a substrate surface. *Appl. Phy. A* **120**, 35–42 (2015).

Acknowledgments: We acknowledge ideaoptics Inc. and M.S. Zhenghong Li for valuable discussion and help in characterizing the optical properties of the printed color pattern. **Funding:** This research is supported by the National Natural Science Foundation of China (grant nos. 22073107, 21522308, 51573192, 51773206, 91963212, and 51961145102), the National Key R&D Program of China (grant nos. 2018YFA0208501 and 2016YFB0401603), the Beijing Natural Science Foundation (grant no. 2194093), the K. C. Wong Education Foundation, and the Beijing National Laboratory for Molecular Sciences (no. BNLMS- CXXM-202005). **Author contributions:** Y.S. and M.L. conceived the project. K.L. performed the experiment with assistance from T.Z., H.L., A.L., Z.L., X.L., X.H., and Y.W. L.S. and T.L. performed the simulations. All the authors discussed the results. K.L., M.L., and Y.S. wrote the paper. All authors proofread the paper, made comments, and approved the manuscript. **Competing interests:** The authors declare that they have no competing interests. **Data and materials availability:** All data needed to evaluate the conclusions in the paper are present in the paper and/or the Supplementary Materials.

Submitted 22 February 2021
Accepted 29 July 2021
Published 22 September 2021
10.1126/sciadv.abh1992

Citation: K. Li, T. Li, T. Zhang, H. Li, A. Li, Z. Li, X. Lai, X. Hou, Y. Wang, L. Shi, M. Li, Y. Song, Facile full-color printing with a single transparent ink. *Sci. Adv.* **7**, eabh1992 (2021).

ScienceAdvances

Facile full-color printing with a single transparent ink

Kaixuan LiTongyu LiTailong ZhangHuizeng LiAn LiZheng LiXintao LaiXiaoyu HouYu WangLei ShiMingzhu LiYanlin Song

Sci. Adv., 7 (39), eabh1992. • DOI: 10.1126/sciadv.abh1992

Science Advances (ISSN) is published by the American Association for the Advancement of Science. 1200 New York Avenue NW, Washington, DC 20005. The title *Science Advances* is a registered trademark of AAAS.